Dynamic redistribution of plasticity in a cerebellar spiking neural network reproducing an associative learning task perturbed by TMS

Alberto Antonietti*[1], Jessica Monaco[2], Egidio D'Angelo[2,3,4], Alessandra Pedrocchi[1] and Claudia Casellato†[1,2]

[1]Department of Electronics, Information and Bioengineering, Politecnico di Milano, Piazza L. da Vinci 32, Milano, Italy
[2]Department of Brain and Behavioral Sciences, University of Pavia, Via Forlanini 6, Pavia, Italy
[3]Brain Connectivity Center, IRCCS C. Mondino, Via Mondino 2, Pavia, Italy
[4]Centro Fermi, Piazza del Viminale 1, Roma, Italy

April 26, 2018

Abstract

During natural learning, synaptic plasticity is thought to evolve dynamically and redistribute within and among subcircuits. This process should emerge in plastic neural networks evolving under behavioral feedback and should involve changes distributed across multiple synaptic sites. In eye-blink classical conditioning (EBCC), the cerebellum learns to predict the precise timing between two stimuli, hence EBCC represents an elementary yet meaningful paradigm to investigate the cerebellar network functioning. We have simulated EBCC mechanisms by reconstructing a realistic cerebellar microcircuit model and embedding multiple plasticity rules imitating those revealed experimentally. The model was tuned to fit experimental EBCC human data, estimating the underlying learning time-constants. Learning started rapidly with plastic changes in the cerebellar cortex followed by slower changes in deep cerebellar nuclei. This process was characterized by differential development of long-term potentiation and depression at individual synapses, with a progressive accumulation of plasticity distributed over the whole network. The experimental data included two EBCC sessions interleaved by a trans-cranial magnetic stimulation (TMS). The experimental and the model response data were not significantly different in each learning phase, and the model goodness-of-fit was > 0.88 for all the experimental conditions. The models fitted on TMS data revealed a slowed down re-acquisition (session-2) compared to the control condition (< 0.01). The plasticity parameters characterizing each model significantly differ among conditions, and thus mechanistically explain these response changes. Importantly, the model was able to capture the alteration in EBCC consolidation caused by TMS and showed that TMS affected plasticity at cortical synapses thereby altering the fast learning phase. This, secondarily, affected also plasticity in deep cerebellar nuclei altering learning dynamics in the entire sensory-motor loop. This observation reveals dynamic redistribution of changes over the entire network and suggests how TMS affects local circuit computation and memory processing in the cerebellum.

1 Introduction

Synaptic plasticity regulates information transmission and processing through neural circuits and is required to drive adaptive behaviors. The cerebellum, the most plastic structure of the brain [1], plays a critical role in adaptive motor control by implementing three fundamental operations: prediction, timing and learning [2, 3, 4]. A mechanistic quantitative interpretation of the dynamic evolution of plasticity during skill acquisition is still lacking, and computational models can be very effective to deal with the issue [5]. An extension of this approach is to perturb the underlying mechanisms, to record the induced behavioral alterations and to tune such a model to generate, and therefore to explain at neural circuit level, the modifications of plasticity dynamics.

It has been shown that a transient interference with the activity of the cerebellar circuit results in an impairment of procedural learning in normal subjects [6]. Transcranial magnetic stimulation (TMS) on the cerebellum is able to

*alberto.antonietti@polimi.it
†claudia.asellato@unipv.it

influence motor control systems, memory, and perception of time [7]. Indeed, cerebellar cortical activity in a restricted time window after training is critical for memory consolidation in keeping with the notion that the cerebellar cortex enables the storage of labile forms of memory into deeper structures [8]. However, the exact mechanisms on which TMS interferes are far from being clear at present.

Eye Blink Classical Conditioning (EBCC) is a Pavlovian associative task, in which the cerebellum learns to predict the precise timing between two stimuli. EBCC training consists in repetitive pairing of a Conditioned Stimulus (CS, like a tone) with an Unconditioned Stimulus (US, like an air-puff or an electrical stimulation) occurring in temporal contiguity and eliciting the eye-blink reflex ("trace" EBCC). The cerebellum learns to produce a Conditioned Response (CR, an eye-blink) precisely timed as to anticipate US onset [9]. The EBCC learning curve is biphasic, according to a two-state model involving a fast and a slow learning process [10, 11]. Recently [12], we have shown that detailed computational cerebellar models can be used to simulate EBCC. However, the available data were insufficient to elaborate a precise hypothesis on the underlying network plastic processes.

A detailed analysis of cerebellar learning and memory consolidation can be performed on EBCC provided that the training paradigms are appropriately designed to capture the underlying kinetic processes and that a causal interference can be applied to disrupt the learning mechanisms at some point (this strategy closely resembles that generally used to investigate dynamic systems, e.g. in electrophysiology [13]). The training paradigms consist of repeated phases of learning, that are differently spaced and can be disturbed by TMS. A two-session EBCC paradigm was initially done with a long washout (1 week) [11, 12], while another design was recently used, applying a short pause (15 minutes) between the first and second training sessions. In both cases, TMS was applied just after the first training session but clearly the two conditions were different in terms of consolidation times [14].

The EBCC data can be mechanistically interpreted through models embedding a well-defined set of learning mechanisms into a detailed cerebellar neural network. A cerebellar Spiking Neural Network (SNN) [15, 16, 17, 18], equipped with distributed plasticity mechanisms [19, 20], was indeed able to translate microcircuit operations occurring over multiple time-scales into the EBCC learning phases [10, 21], reproducing fast acquisition of time-locked motor responses, fast extinction, and memory consolidation. We have extended this approach to the whole set of EBCC data with and without TMS interference on the lateral cerebellum, using enhanced network mechanisms and optimization procedures. This allowed to precisely fit a large set of human EBCC data and formulate a hypothesis, in which learning initiates rapidly in the cerebellar cortex and then proceeds more slowly in deep cerebellar nuclei leading to memory consolidation. This process involves coordinated time-dependent changes in the sign and magnitude of plasticity at multiple synaptic sites, suggesting a much more complex scenario for cerebellar learning than previously thought [22, 23, 4] and revealing the mechanisms of cerebellar TMS interference on learning.

2 Materials and Methods

We used a computational model of the cerebellum, which consisted of a SNN with multiple plasticity mechanisms, and a Genetic Algorithm (GA) for the search of the best models' parameters, in order to reproduce EBCC data collected on human subjects.

EBCC Protocol on Human Subjects

The computational protocol aimed to reproduce the experimental protocol defined by Monaco and colleagues [14]. 36 right-handed healthy subjects participated in this study (21 females and 15 males, mean age 28.6 ± 3.2). Informed consent was obtained from all participants, and the study was approved by the local Ethics Committee and conducted in accordance with regulations laid down in the Declaration of Helsinki. All the human subjects underwent two sessions of EBCC, with a very short pause of 15 minutes between the two sessions. Each session included 6 acquisition blocks of 11 trials each and 1 block of 11 trials of extinction (Figure 1(a)). During the acquisition phase, a CS (a tone) was followed, after an Inter-Stimulus Interval (ISI) of 400 ms, by a US (a supraorbital nerve electric stimulation). During the extinction phase, the subjects received only the CS. CR was detected by EMG recording on the right and left orbicularis oculi muscles. A Magstim Super Rapid magnetic stimulator (MagstimCompany, Whitland, Wales, UK) was used to define the Active Motor Threshold (AMT) and to deliver continuous Theta Burst Stimulation (cTBS). To measure AMT, a figure-of-eight coil was held over the first dorsal interosseous muscle (FDI) hotspot in the left primary motor area (M1). AMT was defined as the lowest intensity able to evoke a MEP of at least 200 μV in five out ten consecutive trials during 10-15% of voluntary contraction of right FDI [24]. cTBS consisting of three-pulse bursts at 50 Hz repeated every 200 ms for 40 s [25] was delivered at 80% AMT (600 pulses) over the lateral hemispheres. A point 1 cm inferior and 3 cm lateral to the inion was stimulated, with the coil handle pointing superiorly, targeting the posterior lobe of the lateral cerebellum [26, 27]. Sham stimulation was delivered with the same intensity as that used in the cTBS protocol but with the coil held perpendicularly to the scalp in order to produce an ineffective cortical activation [28, 29].

All the subjects underwent the first session of the protocol (Figure 1(b)). At the end of the first session, 12 subjects received a sham stimulation, while the other 24 received an effective TMS, 12 on the right and 12 on the left

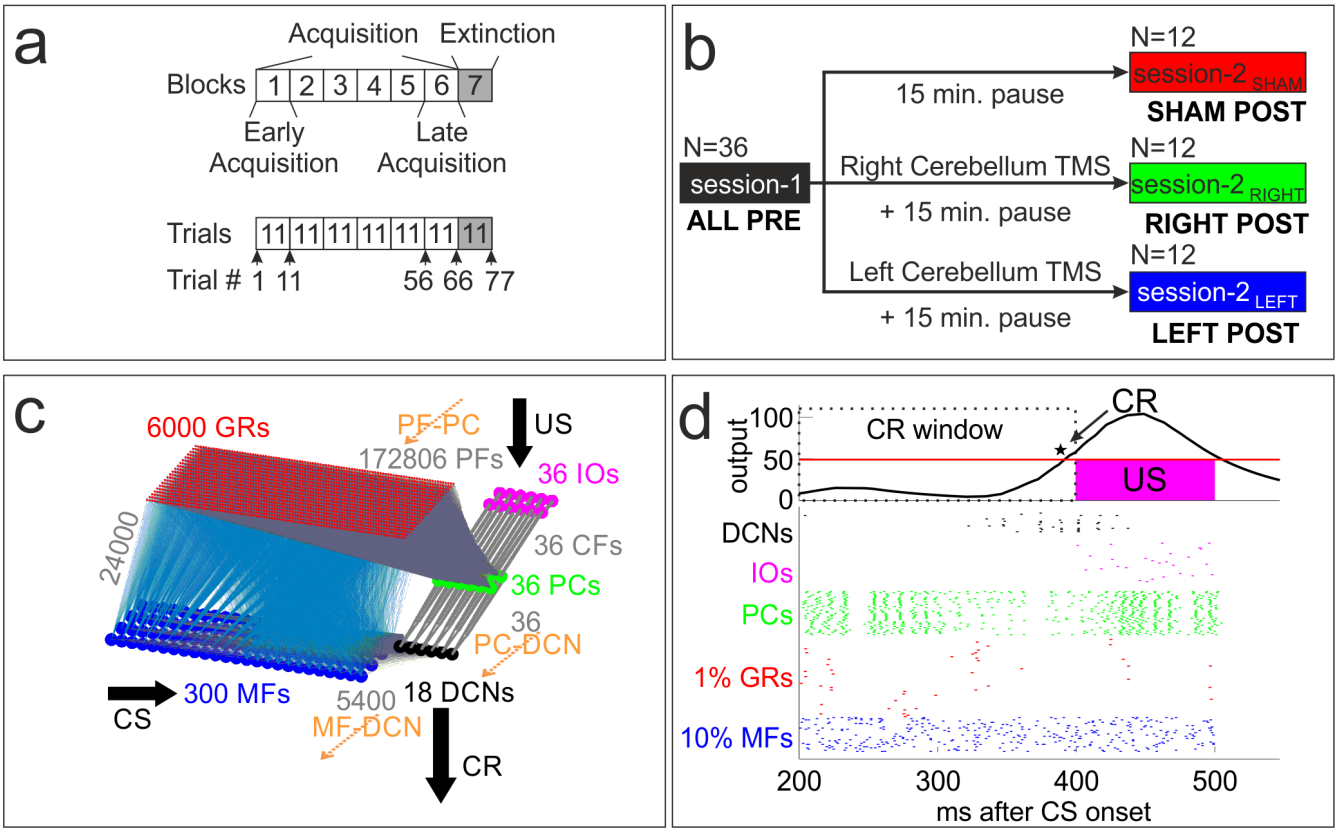

Figure 1: **Experimental protocol and cerebellar model.** **(a)** shows the experimental protocol of one EBCC session. Each block consists of 11 trials, blocks 1-6 were the acquisition blocks, and the 7th was the extinction block (trials 66-77). The first block (trials 1-11) represents the early acquisition, the 6th block (trials 56-66) represents the late acquisition. **(b)** shows the two sessions of the experimental protocol. All the 36 subjects underwent a first session (ALL-PRE), then they were divided into three equal groups of 12 people: SHAM group received a sham TMS stimulation, RIGHT group received an effective TMS stimulation on the right cerebellum, LEFT group an effective TMS stimulation on the left cerebellum. Then they underwent a second EBCC session after 15 minutes of pause. **(c)** shows the architecture of the cerebellar SNN: 300 MFs (blue dots), receiving the CS input signal, 6000 GRs (red dots), 36 PCs (green dots), 36 IOs (magenta dots), receiving the US input signal, 18 DCNs (black dots), which generate the output response. The three plasticity sites are highlighted in orange: the cortical plasticity (PF-PC) and the nuclear plasticities (MF-DCN and PC-DCN). **(d)** shows the raster-plot (the spikes of the different cell populations) of an exemplifying trial (56th) of acquisition in SHAM-POST. For clarity reason, only 10% of MFs (i.e. 30 random MFs) and 1% of the GRs (i.e. 60 random GRs) are depicted. The output signal represents the DCN activity decoded into a control signal, which triggered the CR generation when it overcame the threshold (red line) in the CR windows (from 200 ms before the US onset to the US onset).

hemisphere of the cerebellum. Therefore, the first session (session-1: ALL-PRE) included the data collected from all the 36 subjects; the second sessions (sessions-2: SHAM-POST, RIGHT-POST, and LEFT-POST) included the data recorded from the SHAM, the RIGHT and the LEFT group, respectively (Figure 1(b)).

The numbers of CRs computed for each of the four groups were used for the model fitting as described in the next paragraphs.

Spiking Neural Network Model and Protocol

We exploited a SNN cerebellar model which already proved to be able to reproduce the EBCC protocol in different conditions [20]. The model was simulated by means of EDLUT neural network simulator [30] in order to have accelerated simulations. The SNN mimicked the cerebellar organization, comprising the different populations of neurons, the synaptic connectivity and the learning mechanisms.

The SNN (Figure 1(c)) is made of 6390 Leaky Integrate&Fire neurons [31]: 300 Mossy Fibers (MFs), 6000 Granular cells (GRs), 36 Inferior Olive cells (IOs), 36 Purkinje Cells (PCs) and 18 Deep Cerebellar Nuclei (DCNs). The numbers for each cell type were chosen to resemble the biological ratios [4], as well the electric parameters of the corresponding Integrate&Fire models [32].

MFs and IOs received the input stimuli (CS and US, respectively), GRs made a sparse representation of the input [33, 34] and conveyed through Parallel Fibers (PFs) to PCs, which integrate the information coming from GRs with the signals encoded by IOs. PCs inhibited DCNs, which represented the output of the cerebellum, transmitted to motor neurons. DCNs were in parallel excited by MFs [35].

The convergence/divergence connectivity ratios were taken from neurophysiology. Two kinds of synaptic connections were static (MF-GR and IO-PC), while the other three (PF-PC, MF-DCN and PC-DCN) were plastic. The plastic connections could be classified as cortical for PF-PC, since they extended into the cerebellar cortex, and as nuclear for MF-DCN and PC-DCN, since they involved synapses on Deep Nuclei. Each plastic connection was associated to one plasticity rule that drove its weight changes along time and trials, or increasing the weight by Long Term Potentiation (LTP) or decreasing it by Long Term Depression (LTD). For a detailed description of the learning rules see Supplementary Information and [36, 20]. There are more than 15 forms of synaptic plasticity in the cerebellar network, appearing both as LTP or LTD with multiple and different mechanisms of induction and expression [4]. Understanding the importance of these forms of plasticity and their interplay may greatly benefit from integrated network modeling. However, the model here has been challenged in a simple EBCC task based on timing association; to generate such learning, the cortical plasticity on PCs and the DCN modulation from MF inputs and from PCs themselves are suggested to be the main drivers.

To reproduce the EBCC protocol, the model was fed with *i)* the CS, a MFs random activity of 50 Hz as mean firing rate, lasting 500 ms, and *ii)* the US, a IOs random activity of 1 Hz as mean firing rate, starting after an ISI of 400 ms and lasting 100 ms (thus, co-terminating with the CS). The output activity coming from the DCN was converted into an analog signal using a firing rate based decoding; if the output signal overcame a fixed threshold in a time-window of 200 ms before the US onset, a CR was identified (Figure 1(d)). Every time a CR was detected, the firing rate of the immediately following US was halved (i.e. IOs mean firing rate of 0.5 Hz). During the six acquisition blocks (trials 1-66), the networks received CS-US paired for 10 trials and CS only for the 11th trial of the block. During the extinction block (trials 67-77), the CS only was provided to the network.

Parameter Search by Genetic Algorithm

Meta-heuristic methods for optimization are widely used to find solutions to hard problems, where the search space is complex and poor knowledge about it is available [37]. They are of fundamental interest when dealing with the modeling of complex systems, like brain areas, where automatic procedures become necessary [38]. Classical techniques like gradient-based methods are used to optimize simple neuron models [39, 40], but these algorithms are likely to fail in finding a near-optimal solution for a complex space, because they could stop in a local minimum. Even brute force methods become time-consuming and computationally inefficient. Therefore, metaheuristic methods come out as the best tool to lead fast, efficient and near-optimal tuning of models' parameters. In particular, evolutionary algorithms have been demonstrated to outperform other methods, because they efficiently overcome the trade-off between exploration and exploitation, computational cost and achievement of near-optimal solutions.

As applied in previous works [12, 41, 42, 43], we leveraged a GA to heuristically find the free parameters of the SNN: the initialization weights of the plastic synapses (PF-PC, MF-DCN and PC-DCN) for session-1, and the values of the three pairs of LTP and LTD constants (one pair for each plasticity site) for both session-1 and all the three sessions-2. To find the model reproducing the recorded behavior in session-1, each simulated individual was characterized by a set of 9 parameters (3 initialization weights and 3 pairs of LTP and LTD constants). All the individuals for the sessions-2 did not need initialization weights, since they started with the synaptic weights configuration achieved at the end of session-1. Therefore, for sessions-2, each individual was characterized by a set of 6 parameters (the 3 pairs of LTP and LTD constants). We defined a fitness function, extracting the salient

experimental data features. To optimize the parameters in order to achieve maximal fitness, the whole parameter space was explored. The GA process defining the individuals of the following generation consisted of three parts: selection, crossover, and mutation; explained in detail in Supplementary Information.

Behavioral level: model vs experimental data-set

For the following analyses, we selected the best models which fitted the four datasets. To assure a proper robustness of the results, we did not take into account only one model (the best one) for each group, but we selected a family of good models, considering all the models with a fitness value greater than the 90% of the maximum fitness in that group.

To quantify the goodness of fitting on the experimental data, we compared by Pearson correlation, the median of CR% of human data and the median of model data, along the 77 trials of the protocol, for each of the four groups.

Further, we selected three salient blocks of the protocol: Early Acquisition (EA) (1^{st} block, i.e. trials 1-11); Late Acquisition (LA) (6^{th} block, i.e. trials 56-66) and Extinction (EX) (7^{th} block, i.e. trials 67-77). In these three blocks, we computed the relative number of CRs, as percentage with respect to the maximum number of possible CRs in a single block (i.e. 11). For each group (ALL-PRE, SHAM-POST, RIGHT-POST and LEFT-POST) and for each phase (EA, LA, EX) we applied the Wilcoxon test between the experimental data and the model data, to verify the hypothesis that the two came from the same distribution (i.e. with a $p - value > 0.01$).

Parameters of the models and synapses evolution

The advantage of using models lies in the possibility to shed light on the microscopic mechanisms of the built circuit, responsible for the observed behaviors. The different set of SNN parameters produced the different model behaviors among groups. Thus, we analyzed the LTP and LTD parameters of the four groups, computing their mean and standard deviation, for each of the three plasticity sites. We computed the changes of the parameters in each group's session-2 with respect to the values of session-1. Then, we focused on the differences between the parameters of the two TMS groups and of the SHAM group.

For each group session-2, we computed, for each plastic synapse, the weight changes along trials. Each synaptic change was computed as the value of the weight at the end of each trial with respect to the initial value of that specific weight (i.e. at the beginning of trial 1). These initial values were the same for all sessions-2, because they were the values of the synapses at the end of session-1. Hence, for each of the three plastic sites, we computed the cumulative sum of all the synaptic changes (172 806 connections for PF-PC, 5 400 connections for MF-DCN and 36 connections for PC-DCN), within blocks. This way, each block kept the overall change of the previous one plus the sum of all changes occurring within the 11 trials of that block itself.

Finally, to evaluate the rate of these weight changes, we computed the slopes (m) of the cumulative changes between consecutive blocks. E.g. m1 was the slope computed as the difference between the cumulative sum in block 1 and the initial state, m2 was the difference between the cumulative sum in block 2 and in block 1, and so on.

3 Results

This work can be separated into two main parts: (1) optimization of the model against experimental data and (2) analyses of the microscopic neural features of the models that generated EBCC responses.

Optimization of the model against experimental data

Evaluation of amount of learning

As a first step, model simulations were compared to experimental acquisitions obtained from the four groups: session-1 (ALL-PRE, which works as reference group) and the three different sessions-2: SHAM-POST (with a non-effective TMS) RIGHT-POST and LEFT-POST (with an effective TMS given either to the left or right cerebellar hemisphere). An evolutionary genetic algorithm (GA, see Methods) generated models that closely followed the time course of experimental data. In order to identify a subset of models that could account for inter-subject variability, we identified a family of optimal models in each group. For all groups, the GA produced models with a good fitness in a few hundred generations (for details see Table 1). The near-optimal models generated time courses of EBCC responses (CR%) that overlapped with experimental data (Figure 2(a))

ALL-PRE group. During acquisition, the CR% started from zero and then, after a lag of about 10 trials, increased progressively toward a *plateau* around 70%. During extinction, the CR% rapidly decreased toward zero.

SHAM-POST group. During acquisition, the CR% started from zero and then, with no lag, increased rapidly toward a *plateau* around 80%, i.e. slightly higher than in the ALL-PRE group. During extinction, the CR% rapidly decreased toward zero.

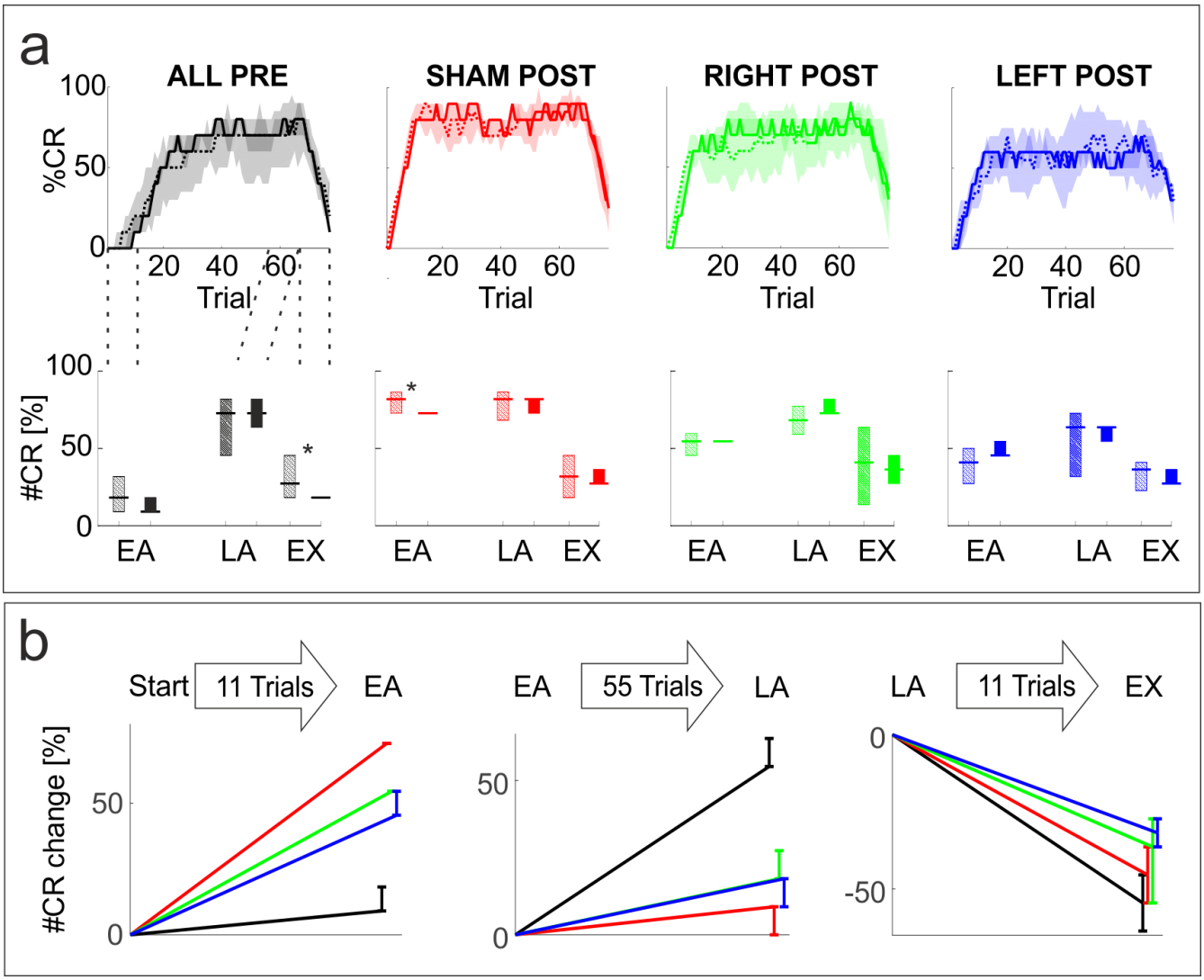

Figure 2: **Model fitting to experimental data. (a)** shows the temporal evolution of learning in the different groups: ALL-PRE (black), SHAM-POST (red), RIGHT-POST (green), LEFT-POST (blue). The graphs show the CR% along the protocol (66 trials of acquisition and 11 trials of extinction, in each group). The dashed lines are experimental data recorded from human subjects, the solid lines and the shaded areas are model data (median and inter-quartile ranges, 25th-75th percentiles). The box-plots show the relative number of CRs in different session phases (median and inter-quartile ranges, 25th-75th percentiles): early acquisition (EA), late acquisition (LA), extinction (EX). Experimental data (hatched boxes) and model data (closed boxes). Asterisks indicate statistical significance of differences between experimental and model data ($p < 0.01$; see Table 1). **(b)** shows changes in the relative number of CRs over the three session phases (median and inter-quartile ranges, 25th-75th percentiles): EA, LA, EX.

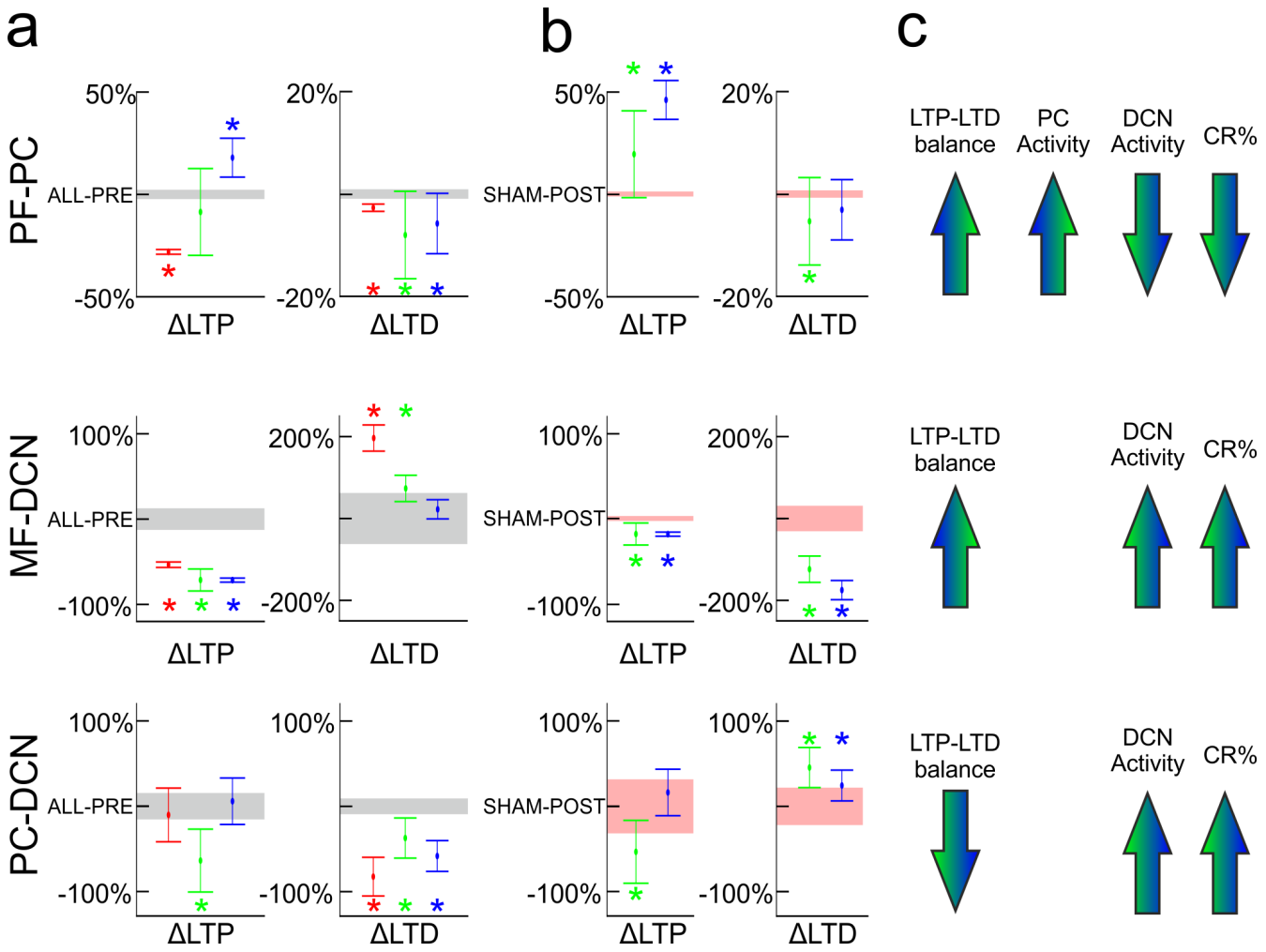

Figure 3: **Difference of plasticity among groups.** **(a)** The bar graphs show, for each plasticity site (PF-PC, MF-DCN and PC-DCN), the changes (ΔLTP and ΔLTD) of each session-2 (mean ± sd) with respect to session-1: ALL-PRE (black band), SHAM-POST (red), RIGHT-POST (green), LEFT-POST (blue). The asterisks indicate significant differences (p ¡ 0.01) from the ALL-PRE group. **(b)** The bar graphs show, for each plasticity site (PF-PC, MF-DCN and PC-DCN), the changes (ΔLTP and ΔLTD) of TMS sessions-2 (mean ± sd) with respect to SHAM-POST: SHAM-POST (red band), RIGHT-POST (green), LEFT-POST (blue). The asterisks indicate significant differences ($p < 0.01$) from the SHAM group. **(c)** shows the effects (overall increase or decrease) of the alterations caused by TMS on the LTP-LTD balance and, consequently, on PC and DCN activity, and on CR generation.

RIGHT-POST and LEFT-POST groups. During acquisition, the CR% started from zero with no lag like in SHAM-POST, but then increased slowly toward a *plateau* around 70%, i.e. slightly lower than in the SHAM-POST group (this difference was more pronounced in the LEFT-POST than in RIGHT-POST). During extinction, the CR% rapidly decreased toward zero but, since the process started from a lower level, the extinction rate was reduced compared to SHAM-POST.

The Pearson correlation coefficient computed between the median CR% of models and the median CR% of experimental data confirmed the goodness of fit for all the four groups (ALL-PRE: $R = 0.97, p < 0.01$; SHAM-POST: $R = 0.94, p < 0.01$, RIGHT-POST: $R = 0.90, p < 0.01$; LEFT-POST: $R = 0.88, p < 0.01$).

An evaluation of learning in specific blocks was performed by comparing the number of CRs between experimental and model data, in three salient phases of the experiment, namely EA, LA and EX phases (Figure 2(a) - second row). Since the data distribution was non-normal, we applied the Wilcoxon test, for each group and each phase). The experimental and the model CR% data were not significantly different ($p > 0.01$), except a slight difference in the EX block of ALL-PRE group and in the EA block of SHAM-POST group (see Table 1). The reason for this can be identified in the very repeatable behavior of the model families, that made the variability across models very small.

Evaluation of learning kinetics

SHAM-POST showed accelerated learning and higher performance compared to ALL-PRE, while RIGHT-POST and LEFT-POST showed slower learning and slower extinction compared to SHAM-POST, suggesting that TMS actually affected some mechanisms of microcircuit plasticity. To quantify the learning kinetics, reflected in the rates of acquisition and extinction, we computed CR variations between specific time points:

1. between the beginning and the end of the fast phases (i.e. the first acquisition block, EA, and the extinction block, EX)

2. between the beginning and the end of the slow phase (i.e. end of the first acquisition block, EA, and end of the last acquisition block, LA).

Learning (early re-acquisition) in sessions-2 turned out to be significantly faster ($p < 0.01$) than in session-1 (Figure 2(b) and Table 2). This was due to a retention of behavior acquired in the first session that facilitated task recalling. Comparing the sessions-2 among each other, the fastest re-acquisition was obtained by the SHAM-POST models, whereas both the RIGHT-POST and the LEFT- POST models were significantly slowed down ($p < 0.01$ vs SHAM-POST).

During later acquisition, after the first block, a slow increase of CR number continued along the next 5 blocks (Figure 2(b)). Such increase was more pronounced in session-1, while sessions-2 showed a lower and slower increase, since a high level of CRs was already present in the first block. Besides the evident difference between session-1 and sessions-2 rates, a higher rate along LA emerged in the TMS groups with respect to the SHAM-POST, especially for one TMS group (RIGHT-POST) compared to the SHAM-POST (Table 2).

During the extinction phase, a slightly reduced speed in CR extinction emerged for the TMS groups, in particular a significant reduction for LEFT-POST compared to SHAM-POST and ALL-PRE (Figure 2(b) and Table 2).

Plasticity parameters in the models

We determined the differences in LTP and LTD parameters at the three plasticity sites (PF-PC, MF-DCN and PC-DCN) that caused the different output behaviors in session-1 and sessions-2. The plasticity parameters, in turn, modulated the activity of PCs and DCN cells and ultimately affected the behavioral performances (the generated CR%).

Cortical plasticity (PF-PC). With respect to the reference values of session-1, the SHAM-POST group showed a substantial decrease of the LTP constant, whereas the RIGHT-POST LTP was slightly diminished and the LEFT-POST LTP was even increased (Figure 3(a)). The LTD value of SHAM-POST was almost unvaried, whereas the LTD values of both the TMS groups were considerably diminished. As global effect, when comparing the unaltered conditions (ALL-PRE vs SHAM-POST), cortical synapses in the session-2 showed stronger depression, decreasing PC activity and facilitating CR generation. This was consistent with the faster early acquisition rate observed in sessions-2 (especially in the SHAM-POST) compared to session-1 (Figure 2(a)). When comparing sessions-2, one with each other (TMS groups vs SHAM-POST), the TMS effect was reflected by a general increase in the LTP and a decrease of the LTD constants, hence increasing PC activity and decreasing DCN activity (Figure 3(b)). As a result, the CR generation in the TMS groups was slowed down, especially in the fast processes where cortical plasticity was more critically involved (Figure 3(c)).

Nuclear plasticity between MF and DCN. With respect to the reference values of session-1, all the three sessions-2 showed a decrease of the LTP constant; the SHAM-POST LTD constant was reinforced, whereas the LTD values of the TMS groups were essentially unvaried (Figure 3(a)). This was consistent with a lower CR slow increase along the

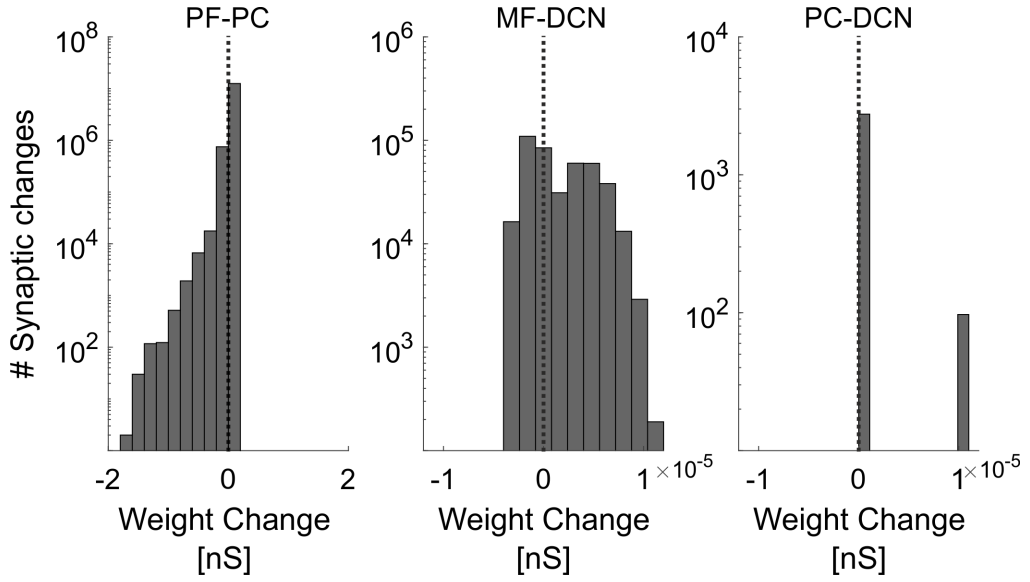

Figure 4: **Evolution of individual synaptic weights along trials.** Histogram of changes of each synaptic weight, between all consecutive trials during session-2 in SHAM-POST, for each plasticity site (PF-PC, MF-DCN and PC-DCN).

whole acquisition observed in sessions-2 compared to session-1 (Figure 2(b)). When comparing sessions-2, one with each other (TMS groups vs SHAM-POST), the LTP parameter was more strongly decreased and the LTD parameter was less increased in the TMS groups than in the SHAM-POST group (Figure 3(b)). Therefore, the global effect was an increased excitability of DCNs from the MF input. As a result, the CR generation in the TMS groups was slightly fostered, but on a slow time-scale since the nuclear plasticity had a slow dynamics (Figure 3(c)).

Nuclear plasticity between PC and DCN. With respect to the reference values of session-1, the SHAM-POST and the LEFT-POST LTP constants did not change, whereas the RIGHT-POST LTP was strongly decreased. All sessions-2 showed reduced LTD constants (Figure 3(a)). As global effect, this plasticity in sessions-2 was more inclined to be potentiated, thus with a stronger inhibition on the output. Analogously to the other nuclear plasticity (described above), this was consistent with a lower CR slow increase along the whole acquisition observed in sessions-2 compared to session-1 (Figure 2(b)). When comparing sessions-2, one with each other (TMS groups vs SHAM-POST), the LTD constants of the TMS groups were decreased of a lower amount than in SHAM-POST (Figure 3(b)). Therefore, the global TMS effect was a weaker inhibition from PCs on DCNs, thus augmenting DCN activity. As a result, the CR generation in the TMS groups was slightly fostered, but on a slow time-scale since the nuclear plasticity had a slow dynamics (Figure 3(c)). Any improvement in performance in session-2 compared to session-1 could be due to two factors, i) the initial weight configuration not naïve but achieved after a first training, and ii) the remodulation of LTP-LTD balances.

Therefore, the main TMS effect was to slow down the fast CR generation driven by cortical cerebellar plasticity (in the models, it corresponds to an unwanted facilitation of the synapses from PFs to PCs and thus a counter-productive inhibition on DCN output activity). This TMS-induced deficit triggered a compensatory action of the nuclear plasticity sites to partially counterbalance the weakness of those cortical mechanisms in producing associative responses, throughout a reinforcement of DCN activity. As a drawback, these indirect TMS effects on nuclear mechanisms, since reversing them takes longer, might slow down the fast unlearning process required in extinction (extinction rate).

Dynamic evolution of plasticity along trials at multiple synapses

Learning is the consequence of the synaptic changes of the individual connections in the three plasticity sites, with different amplitude and speed. Each synaptic connection had its own time course, but the behavioral output depends on the overall weight configuration. The PF-PC and MF-DCN synapses did not behave in the same way (Figure 4). Actually, more mechanisms coexist so that the variety of behavior may be even higher. On the other hand, PC-DCN synapses were homogeneously and monotonically modulated. However the behavioral output depends on the overall weight configuration. The effects of the modifications of the LTP-LTD balance in the sessions-2 (Figure 3 (b) and (c)) can be seen in the evolution of synaptic strengths. Starting from the same initial weight configuration (the end of session-1), the cortical and nuclear weight changes accumulated differently along trials between SHAM and TMS sessions (Figure 5).

Cortical plasticity (PF-PC). Along the 6 acquisition blocks, the cortical synapses accumulated strength decreases

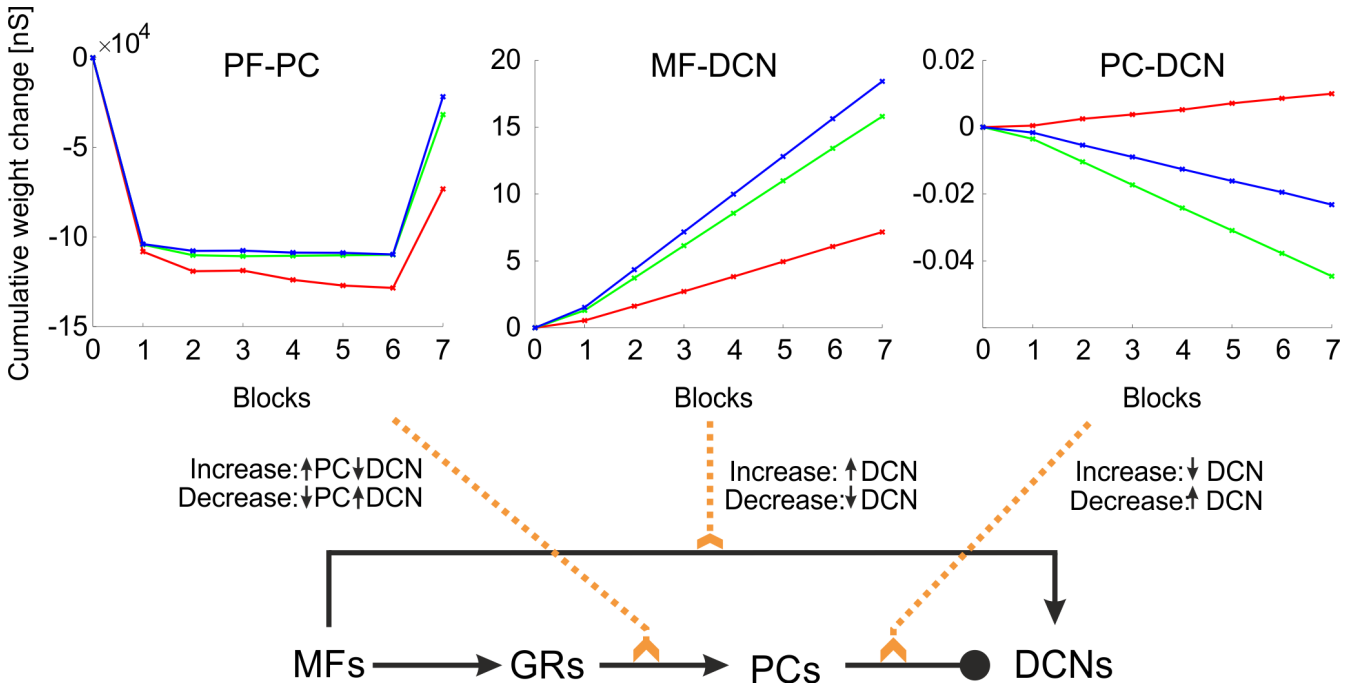

Figure 5: **Evolution of synaptic weights along blocks.** Cumulative changes of synaptic weights along sessions-2: SHAM-POST (red), RIGHT-POST (green), LEFT-POST (blue). The weights evolve from initial values corresponding to those attained by the end of the session-1 for the three plasticity sites. The slopes of the straight segments between consecutive blocks are reported in Table 3. The scheme represents the influence of weight changes on the cerebellar circuitry, highlighting the effects of the synaptic changes on the output neural responses of DCNs.

in favor of CR generation (weaker excitation from PFs to PCs); the strongest strength change was in the first block, then very small modulation occurred (Figure 5). In details, TMS curves had a smaller slope in the first block (m1) than the SHAM curve; also, the successive additive modulations along acquisition blocks were smaller than in SHAM (Table 3). In extinction, the cortical synaptic strength was changed in the reverse direction (positive slopes m7). However, TMS curves showed a faster weight increase since their LTP-LTD balance was more in favor of DCN inhibition (required for extinction).

Nuclear plasticity between MF and DCN. These nuclear synapses accumulated strength increases in favor of CR generation (stronger overall excitation to DCNs) (Figure 5). They showed a continuous slight increase of accumulated weight change along trials (e.g. m1 lower than m2). TMS curves had higher slopes among all acquisition blocks, compared to SHAM. In the extinction block, the nuclear synaptic modulation went through a slowdown (m7 $<$ m6), but without a sudden reverse (m7 still positive). This was consistent with the observed reduction of the extinction speed in TMS groups, for which MF-DCN synapses achieved a more relevant role in CR generation during late acquisition. However, this side effect was quite mitigated by cortical plasticity more moved to LTP, than in SHAM condition.

Nuclear plasticity between PC and DCN. These synapses changed their weights in different directions when comparing sessions-2 among each other. For the SHAM-POST group the synapses accumulated strength changes increasing the inhibition of PCs over DCNs (Figure 5). For the TMS groups, the synapses decreased the inhibition strength of PCs over DCNs. This is coherent with the changes, for this plasticity site, in LTP-LTD parameters between SHAM and TMS groups. While the MF-DCN plasticity had an overall modulatory effect, generally increasing the DCN firing, the PC-DCN plasticity was needed for sharpening the DCN activity, avoiding the co-activation of DCNs while PCs were still firing. However, this plasticity, among the three, was the least influential on the CR generation process, since the changes in the synaptic weights were marginal.

4 Discussion

In this paper, a modeling reconstruction of the cerebellar circuit, based on a spiking neural network, has been successfully used to fit experimental human data of EBCC learning. The main result is that the model was able to capture the EBCC alterations caused by transcranial magnetic stimulation (TMS) and to suggest an explanation of the underlying microcircuit mechanisms. An accurate analysis of model parameters, during different phases of the EBCC learning paradigm, showed that the main effect of TMS was to alter plasticity at cortical synapses. This happened by impairing a fast mechanism of learning located in the cerebellar cortex, that has been identified with

plasticity at the parallel fiber - Purkinje cell synapses. As a reflection of this change in cortical plasticity, plasticity was altered also in the deep cerebellar nuclei. This observation provides the first mechanistic explanation of how TMS might affect local circuit computation and memory processing in the cerebellum.

Specific properties of the modeling approach

There are three aspects of this modeling approach that are worth being considered:

1. The model incorporates a spiking neural network in an extended sensori-motor loop. This architecture exploits an implicit computational process that was not designed a priori for the purpose but rather reflects the natural properties of the cerebellar network. Such an approach is bottom-up and informs us about the mechanisms that allow the cerebellum, inside a sensori-motor loop, to control behavior. An improvement of biophysical details describing network mechanisms (e.g. neural properties [44], synaptic transmission and plasticity rules [45]) would allow gaining further insights into the elementary bases of cerebellar learning.

2. The model, by being free of assumptions on the target function and by implementing realistic neural mechanisms, allowed to simulate different behaviors, of which EBCC is just one specific case [46, 47, 48].

3. The model exploited an automatic parameterization of network plasticity mechanisms. This allowed it to tune against specific datasets, reflecting states in which learning showed modifications, e.g. after TMS. Model simulations uncovered remarkable changes in the LTP-LTD balance at the three plasticity sites of the network following TMS.

Mechanisms underlying learning in the model

As far as the mechanisms of cerebellar learning are concerned, these occur through a modulation of the weights at individual synapses, with site-specific LTP-LTD balances. This, eventually, impacts on the cumulative changes causing learning along trials. The changes occurred both at PF-PC and at PC-DCN and MF-DCN synapses, although with several differences.

First, the multiple plasticity rules, which were derived from experimental indications [49], imposed higher weight rate at the PF-PC than at PC-DCN or MF-DCN synapses. This allowed patterns to be stored rapidly into the cerebellar cortex and subsequently to be stabilized in the DCN [50].

Secondly, while there was a general trend toward LTD in the cortex and toward LTP in the nuclei, individual synapses could sometimes show opposite changes (e.g. some cortical synapses showed LTP rather than LTD) as well as different intensity or rate of change. While learning was progressing, some synapses could go in a direction opposite to the cumulative changes in synaptic weights. This effect was most evident in PF-PC and PC-DCN synapses. It follows that, in recordings *in vivo* one should not expect to observe homogeneous and monotonic changes in all the synapses of a given kind during a behavioral learning task.

Thirdly, plasticity at PF-PC was directly supervised by IO, plasticity at PC-DCN was driven by the relative timing between pre and post synaptic activity, and MF-DCN synapses influenced the DCN overall excitability supervised by PC activity ([51]; for review see [52]), such that high PC activity favors MF-DCN LTD and *vice versa*. Eventually, in the EBCC paradigm, PF-PC and PC-DCN synapses were mostly responsible for determining response timing and MF-DCN synapses for regulating output intensity, implementing a combined phase and gain modulator. Therefore, synergism and inter-dependency among distributed plasticity sites characterized the cerebellar learning dynamics, where the nuclear synapses supported in the long-term and refined the faster cortical operations.

It should be noted that, according to plasticity rules (see Methods; [53]), the IO signal was a primary driver for plasticity, as predicted by the original Marr's model [22]. The situation may be somehow different if other forms of plasticity were also included. E.g. plasticity in the granular layer, that was not considered here, may involve different control mechanisms [54] and generate additional phase and gain regulation at the cerebellar cortex input stage.

Recent literature suggests a form of learning involving an intrinsic cellular timing mechanism (e.g. receptor-mediated postsynaptic inhibition in PCs during EBCC), besides the long-term plasticity generating changes in synaptic strengths [55]. Our approach uses a simplified computational model which does not take into account neuron sub-cellular mechanisms, able to express this intrinsic receptor-based modulation. However, in future extensions, more detailed neuron models equipped with molecular mechanisms could be embedded into the network model. Moreover, in future extensions, the learning rules could be extended and enhanced in order to impose a change level on each synaptic connection also depending on its individual actual strength.

Network changes underlying TMS-induced learning alterations

Cerebellar function is increasingly investigated with neurostimulation techniques such as TMS [56]. A wide range of different protocols exists, the coil geometry and stimulation intensity have a considerable impact on the efficacy of TMS stimulation. In investigating cerebellar-cortex loop, inhibitory repetitive TMS (rTMS) on cerebellum was

used to induce a "virtual lesion" and evaluate the physiological effects on excitability of the primary motor cortex [57, 58, 27, 59]. Pinto and colleagues [60] showed how conditioning magnetic stimulation of the cerebellum suppresses the motor cortex 5–8 ms later (decrease of the TMS-induced motor-evoked potential), probably through activation of cerebellar PCs, which inhibit the dentate-thalamo-cortical pathway; double-cone coil was centered 3 cm lateral to the inion for right cerebellar stimulation. Other studies used rTMS to disrupt function in the right cerebellum, a region implicated in language, thus extending the cerebellar theory of predictive motor control to the non-motor cerebellum [61].

rTMS is capable of producing long-lasting alterations in plasticity; this means potential uses of rTMS as a therapeutic tool producing effects e.g on the cerebral cortex that outlast the stimulus. It is still not clear how much durable are the TMS-induced plasticity changes; these phenomena may represent precursors of LTD and LTP [62]. In this context, for instance, studies exploring the combination of TMS and dopaminergic agents in an effort to enhance synaptic plasticity and improve function in patients with chronic stroke are underway. Our approach uses a simplified computational model which does not take into account neuron morphologies and sub-cellular mechanisms; therefore, it does not allow to explore such level of details.

The main observation in this work is that cerebellar cTBS delivered a few minutes after EBCC training can interfere with the early phase of memory consolidation tested soon thereafter. This finding extends initial observations in which the effects of cerebellar cTBS on EBCC were tested with less stringent temporal constraints [63, 11]. In a first investigation [63] cerebellar cTBS was applied before EBCC training and the effect was verified after one week. This protocol caused a lower number of CRs compared to unstimulated subjects. This seminal work revealed that cTBS could indeed impair CRs in EBCC "in some way", but left open the questions on whether acquisition or retention were impaired and of where and how the impairment occurred. In a second investigation [11], cerebellar cTBS was applied after EBCC training and again the effect was verified after one week. This second protocol caused a slowing down of the extinction phase compared to unstimulated subjects, suggesting that a rapid process was selectively altered, but again the impact of cTBS on subsequent consolidation remained unexplored. Therefore, given these major missing elements, in the present paper we have tested TMS interference during the memory transfer time-window. We discuss the found effects dependent on the time frame at which the cTBS interferes with the learning and consolidation processes. Other time frames for interference could perturb the slope of the ongoing acquisition or the maintenance of response generation.

The presented simulations showed that plasticity acquired during an initial training session (session-1) was important to accelerate learning during the next session (session-2). This maintenance of plasticity could therefore explain the retention of learning through the intervention of some yet unknown consolidation processes. Indeed, plasticity should be naturally extinguished within tens of minutes, since it is reversible both at nuclear (about 60 minutes) and PF-PC synapses (about 10 minutes). This fact was already obvious in our previous study, in which the time between sessions 1 and 2 was one week [11].

TMS disrupted this consolidation even when delivered just after session 1, indicating that the consolidation process started very early during training. In particular, slowing down of the fast reacquisition and extinction phases indicated a damage to the fast learning process. Our simulations suggest that cerebellar TMS interfered with the dynamic acquisition of motor memory by modifying LTP-LTD balances. This impaired the process that would normally reduce PC activity and dis-inhibit DCN. The nuclear plasticities underwent modifications facilitating the DCN output, therefore providing a (partial) compensation for the exceeding inhibition provided by the cortex. On a slow time-scale, the nuclear mechanisms summed their effects to cortical ones, eventually recovering CR generation toward the normal steady-state level.

In our previous work [12], models were tuned on a two- sessions EBCC human dataset, with a long washout (1 week) and TMS was administrated over the right lateral cerebellum at the end of the first session. In that protocol, the only phase compromised in the TMS group was the extinction, while the fast recalling of learned associations in early acquisition was intact. When comparing those findings with the results shown here, it could be inferred that the long washout allowed a reorganization of plasticity, such that leaned associations were consolidated. On the other hand, with a short pause (this dataset) such reorganization process had not time to complete and task recalling was compromised. This interpretation supports the concept that memory consolidation starts as early as during acquisition and can be altered by interference during ongoing learning or just thereafter. The involvement of the cerebellar cortex in EBCC was previously suggested by experiments in which the GABAa receptor agonist muscimol was infused to transiently inactivate local circuit functions in rats. Infusion of muscimol in the posterior cerebellar cortex (lobule HVI) was effective after short (5-45 min) [64] but not after longer delays (90 min) [65]. Conversely, muscimol infusion in the anterior interpositus nucleus just after training was poorly effective. These experiments suggested that learning was transferred quite early from a cortical into a nuclear neuronal site. Therefore, here we have tested TMS interference during the memory transfer time-window.

From a methodological point of view, with respect to our previous work [12], we have scaled-up the computational model in order to achieve a better encoding/decoding resolution. Finally, we have made the cost function of the optimization procedure more complete by taking into account all the learning phases. Therefore, the model has now reached maturity and has allowed to account for all the data reported in this and the previous works.

Circuit modeling as a tool for understanding the basis of learning and its alterations

Circuit modeling, combined with a non-invasive perturbation of neural circuits, could be useful to investigate a wide range of circuit (dys)functions during behavior, due to imposed neural interferences or to specific diseases. TMS interference with the activity of the lateral cerebellum induced a significant decrease in procedural learning, i.e. in the acquisition of motor skills through repeated performance and practice [6]. In particular here we infer the TMS-induced alterations which become evident in the slowing down of the fast acquisition processes. Conversely, anodal tDCS (transcranial Direct Current Stimulation) of the cerebellum substantially increased the rate of adaptation [66] Misbehaviors can also occur due to cerebellar diseases [67]; for example, patients with cerebellar ataxia are severely impaired in compensating for systematic perturbations and the adaptation deficits in cerebellar lesions are due to a reduced sensitivity to prediction errors [50]. In all these and other cases, computational modeling could provide a mechanistic interpretation of the underlying plasticity and neural activity changes [68, 69, 70].

Our model has been tuned on dataset in which TMS interference was delivered on right or on left cerebellum. This may suggest cues about inter-hemispheric differences in the lateral cerebellum. Previous works [6] suggested that the right cerebellum was more involved than its twin in implicit learning of new sequences through both hands. This was proposed to reflect asymmetric connections with the contralateral parietal cortex [71], consistent with the dominance of the left cerebral cortex in movement control. In this work, although TMS on the left seemed to interfere more than that on the right cerebellum, the difference was not significant, suggesting that EBCC learning has bilateral control. However, anatomo-clinical studies have not been able to provide a coherent picture with regard to lateralization nor localization of the causative lesion within the cerebellum [72]. Further studies are warranted to address this issue.

5 Conclusion

In conclusions, this work shows that a macroscopic measurement during a behavioral task can be successfully explained by using an appropriate model constructed at the microscopic level, i.e. using a bio-inspired neural network derived from physiological and anatomical data. In particular, we have been able to tune a spiking cerebellar neural network model against human EBCC data before and after perturbation with TMS

The emerging view is that cerebellar plasticity is a dynamic and distributed process, in which cortical plasticity is more rapidly activated and drives a set of changes that reverberate onto the more slowly adapting DCN. Changes or deficiencies occurring in one site are compensated by the others suggesting possible interventional sites for therapy and repair. This result bears a series of consequences. First, an approach similar to that used here for TMS could be exploited to understand the yet unknown mechanisms of action of other interventional techniques, e.g. tDCS or TES (Transcranial Electrical Stimulation), which are more and more widely used for investigation, diagnosis and treatment of brain diseases. Secondly, application of this approach to brain pathologies could provide a further understanding of their pathophysiological mechanisms. The predictions of these models are warranted future experimental investigations, e.g. performing *in vivo* multi-electrode recordings of the plastic evolution of neural discharges in cortical and deep cerebellar nuclei neurons during EBCC tests [73].

In silico simulations based on realistic computational modeling and tuned on experimental data could become fundamental to formulate hypotheses on disease mechanisms and to evaluate the efficacy of treatments and estimate the expected recovery time evolution. This approach may eventually lead to design new diagnostic and therapeutic tools addressing the concepts of personalized medicine in neurorehabilitation.

Data availability

The data that support the findings of this study and the scripts to reproduce all the figures and tables are available in Harvard Dataverse with the identifier doi:10.7910/DVN/KW88YE

Acknowledgments

This project has received funding from the European Union's Horizon 2020 Framework Programme for Research and Innovation under Grant Agreement No. 720270 (Human Brain Project SGA1) and by the HBP Partnering Project cerebNEST.

References

[1] Rodolfo Llinas and Mario Negrello. Cerebellum. *Scholarpedia*, 10(1):4606, 2015.

[2] Silvia Tolu, Mauricio Vanegas, Jesús A Garrido, Niceto R Luque, and Eduardo Ros. Adaptive and predictive control of a simulated robot arm. *International journal of neural systems*, 23(3):1350010, 6 2013.

[3] Egidio D'Angelo, Sergio Solinas, Jesus Jesús A Garrido, Claudia Casellato, Alessandra Pedrocchi, Jonathan Mapelli, Daniela Gandolfi, and Francesca Prestori. Realistic modeling of neurons and networks: towards brain simulation. *Functional neurology*, 28(3):153–166, 2013.

[4] Egidio D'Angelo, Alberto Antonietti, Stefano Casali, Claudia Casellato, Jesús A Garrido, Niceto R Luque, Lisa Mapelli, Stefano Masoli, Alessandra Pedrocchi, Francesca Prestori, Martina F Rizza, and Eduardo Ros. Modeling the Cerebellar Microcircuit: New Strategies for a Long-Standing Issue. *Frontiers in Cellular Neuroscience*, 10(July):176, 2016.

[5] Romain Brette, Michelle Rudolph, Ted Carnevale, Michael Hines, David Beeman, James M. Bower, Markus Diesmann, Abigail Morrison, Philip H. Goodman, Frederick C. Harris, Milind Zirpe, Thomas Natschläger, Dejan Pecevski, Bard Ermentrout, Mikael Djurfeldt, Anders Lansner, Olivier Rochel, Thierry Vieville, Eilif Muller, Andrew P. Davison, Sami El Boustani, and Alain Destexhe. Simulation of networks of spiking neurons: A review of tools and strategies. *Journal of Computational Neuroscience*, 23(3):349–398, 12 2007.

[6] Sara Torriero, Massimiliano Oliveri, Giacomo Koch, Carlo Caltagirone, and Laura Petrosini. Interference of Left and Right Cerebellar rTMS with Procedural Learning. *Journal of Cognitive Neuroscience*, 16(9):1605–1611, 2004.

[7] Eduard Minks, Marie Kopickova, Radek Marecek, Hana Streitova, and Martin Bares. Transcranial magnetic stimulation of the cerebellum. *Biomed Pap Med Fac Univ Palacky Olomouc Czech Repub*, 154(2):133–139, 2010.

[8] Daniel O. Kellett, Izumi Fukunaga, Eva Chen-Kubota, Paul Dean, Christopher H. Yeo, and P Dean. Memory Consolidation in the Cerebellar Cortex. *PLoS ONE*, 5(7):e11737, 7 2010.

[9] Javier F Medina and Michael D Mauk. Computer simulation of cerebellar information processing. *Nature neuroscience*, 3 Suppl(SUPPL.):1205–11, 11 2000.

[10] Maurice A Smith, Ali Ghazizadeh, and Reza Shadmehr. Interacting adaptive processes with different timescales underlie short-term motor learning. *PLoS biology*, 4(6):e179, 6 2006.

[11] Jessica Monaco, Claudia Casellato, Giacomo Koch, and Egidio D'Angelo. Cerebellar theta burst stimulation dissociates memory components in eyeblink classical conditioning. *The European journal of neuroscience*, 40(July):1–8, 9 2014.

[12] Alberto Antonietti, Claudia Casellato, Egidio D'Angelo, and Alessandra Pedrocchi. Model-driven analysis of eyeblink classical conditioning reveals the underlying structure of cerebellar plasticity and neuronal activity. *IEEE Transactions on Neural Networks and Learning Systems*, PP(99):1–15, 9 2016.

[13] Eugene M Izhikevich. *Dynamical systems in neuroscience : the geometry of excitability and bursting*. MIT Press, 2007.

[14] Jessica Monaco, Lorenzo Rocchi, Egidio D'Angelo, and John C Rothwell. Cerebellar theta burst stimulation impairs memory consolidation in eye-blink classical conditioning. *Submitted*, 2017.

[15] Samanwoy Ghosh-Dastidar and Hojjat Adeli. Spiking neural networks. *International journal of neural systems*, 19(4):295–308, 8 2009.

[16] Samanwoy Ghosh-Dastidar and Hojjat Adeli. A new supervised learning algorithm for multiple spiking neural networks with application in epilepsy and seizure detection. *Neural Networks*, 22(10):1419–1431, 12 2009.

[17] Linqiang Pan, Gheorghe Păun, Gexiang Zhang, and Ferrante Neri. Spiking Neural P Systems with Communication on Request. *International Journal of Neural Systems*, 27(08):1750042, 12 2017.

[18] Simeon Knieling, Kousik S. Sridharan, Paolo Belardinelli, Georgios Naros, Daniel Weiss, Florian Mormann, and Alireza Gharabaghi. An Unsupervised Online Spike-Sorting Framework. *International Journal of Neural Systems*, 26(05):1550042, 8 2016.

[19] Eduardo Ros, Richard R Carrillo, Eva M Ortigosa, Boris Barbour, and Rodrigo Agís. Event-driven simulation scheme for spiking neural networks using lookup tables to characterize neuronal dynamics. *Neural computation*, 18(12):2959–93, 12 2006.

[20] Alberto Antonietti, Claudia Casellato, Jesús A Garrido, Niceto R Luque, Francisco Naveros, Eduardo Ros, Egidio DAngelo, Alessandra Pedrocchi, Egidio D'Angelo, and Alessandra Pedrocchi. Spiking Neural Network With Distributed Plasticity Reproduces Cerebellar Learning in Eye Blink Conditioning Paradigms. *IEEE Transactions on Biomedical Engineering*, 63(1):210–9, 1 2016.

[21] Claudia Casellato, Alberto Antonietti, Jesús A Garrido, Giancarlo Ferrigno, Egidio D'Angelo, and Alessandra Pedrocchi. Distributed cerebellar plasticity implements generalized multiple - scale memory components in real - robot sensorimotor tasks. *Frontiers in Computational Neuroscience*, 9, 2 2015.

[22] David Marr. A theory of cerebellar cortex. *The Journal of physiology*, 202(2):437–70, 6 1969.

[23] James S Albus. A theory of cerebellar function. *Mathematical Biosciences*, 10(1-2):25–61, 2 1971.

[24] P M Rossini, A T Barker, A Berardelli, M D Caramia, G Caruso, R Q Cracco, M R Dimitrijević, M Hallett, Y Katayama, and C H Lücking. Non-invasive electrical and magnetic stimulation of the brain, spinal cord and roots: basic principles and procedures for routine clinical application. Report of an IFCN committee. *Electroencephalography and clinical neurophysiology*, 91(2):79–92, 8 1994.

[25] Ying-Zu Huang, Mark J. Edwards, Elisabeth Rounis, Kailash P. Bhatia, and John C. Rothwell. Theta Burst Stimulation of the Human Motor Cortex. *Neuron*, 45(2):201–206, 1 2005.

[26] Miguel Fernandez Del Olmo, Binith Cheeran, Giacomo Koch, and John C. Rothwell. Role of the Cerebellum in Externally Paced Rhythmic Finger Movements. *Journal of Neurophysiology*, 98(1):145–152, 7 2007.

[27] G. Koch, M. Oliveri, B. Cheeran, D. Ruge, E. L. Gerfo, S. Salerno, S. Torriero, B. Marconi, F. Mori, J. Driver, J. C. Rothwell, and C. Caltagirone. Hyperexcitability of parietal-motor functional connections in the intact left-hemisphere of patients with neglect. *Brain*, 131(12):3147–3155, 12 2008.

[28] Livia Brusa, Roberto Ceravolo, Lorenzo Kiferle, Fabrizia Monteleone, Cesare Iani, Orazio Schillaci, Paolo Stanzione, and Giacomo Koch. Metabolic changes induced by theta burst stimulation of the cerebellum in dyskinetic Parkinson's disease patients. *Parkinsonism & related disorders*, 18(1):59–62, 1 2012.

[29] Giacomo Koch, Diane Ruge, Binith Cheeran, Miguel Fernandez Del Olmo, Cristiano Pecchioli, Barbara Marconi, Viviana Versace, Emanuele Lo Gerfo, Sara Torriero, Massimiliano Oliveri, Carlo Caltagirone, and John C Rothwell. TMS activation of interhemispheric pathways between the posterior parietal cortex and the contralateral motor cortex. *The Journal of physiology*, 587(Pt 17):4281–92, 9 2009.

[30] Eduardo Ros, Eva M Ortigosa, Rodrigo Agís, Richard R Carrillo, and Michael Arnold. Real-time computing platform for spiking neurons (RT-spike). *IEEE Transactions on Neural Networks*, 17(4):1050–1063, 2006.

[31] Phill Rowcliffe and Jianfeng Feng. Training spiking neuronal networks with applications in engineering tasks. *IEEE Transactions on Neural Networks*, 19(9):1626–1640, 2008.

[32] Niceto R Luque, Jesús A Garrido, Richard R Carrillo, Silvia Tolu, and Eduardo Ros. Adaptive cerebellar spiking model embedded in the control loop: context switching and robustness against noise. *International journal of neural systems*, 21(5):385–401, 10 2011.

[33] Guy Billings, Eugenio Piasini, Andrea Lorincz, Zoltan Nusser, Andrea Lőrincz, Zoltan Nusser, and R Angus Silver. Network Structure within the Cerebellar Input Layer Enables Lossless Sparse Encoding. *Neuron*, 83(4):960–974, 8 2014.

[34] Andrea Giovannucci, Aleksandra Badura, Ben Deverett, Farzaneh Najafi, Talmo D Pereira, Zhenyu Gao, Ilker Ozden, Alexander D Kloth, Eftychios Pnevmatikakis, Liam Paninski, Chris I De Zeeuw, Javier F Medina, and Samuel S-H Wang. Cerebellar granule cells acquire a widespread predictive feedback signal during motor learning. *Nat Neurosci*, advance on, 3 2017.

[35] Niceto R Luque, Jesús A Garrido, Jarno Ralli, Juanlu J Laredo, and Eduardo Ros. From sensors to spikes: evolving receptive fields to enhance sensorimotor information in a robot-arm. *International journal of neural systems*, 22(04):1250013, 8 2012.

[36] Jesús A. Garrido, Niceto R. Luque, Egidio D'Angelo, and Eduardo Ros. Distributed cerebellar plasticity implements adaptable gain control in a manipulation task: a closed-loop robotic simulation. *Frontiers in neural circuits*, 7(October):159, 1 2013.

[37] Stefan Voß. Meta-heuristics: The State of the Art. In Alexander Nareyek, editor, *Local Search for Planning and Scheduling*, volume 2148 of *Lecture Notes in Computer Science*, pages 1–23. Springer Berlin Heidelberg, Berlin, Heidelberg, 10 2001.

[38] Werner Van Geit, Erik De Schutter, and Pablo Achard. Automated neuron model optimization techniques: a review. *Biological Cybernetics*, 99(4-5):241–251, 11 2008.

[39] M C Vanier and J M Bower. A comparative survey of automated parameter-search methods for compartmental neural models. *Journal of computational neuroscience*, 7(2):149–71.

[40] Joseph H. Tien and John Guckenheimer. Parameter estimation for bursting neural models. *Journal of Computational Neuroscience*, 24(3):358–373, 6 2008.

[41] Kristofor D Carlson, Jayram M Nageswaran, Nikil Dutt, and Jeffrey L Krichmar. An efficient automated parameter tuning framework for spiking neural networks. *Frontiers in neuroscience*, 8(February):10, 1 2014.

[42] Robert Batllori, Craig B Laramee, Walker H Land, and J David Schaffer. Evolving spiking neural networks for robot control. *Procedia Computer Science*, 6(0):329–334, 1 2011.

[43] Stefan Schliebs, Michaël Defoin-Platel, Sue Worner, and Nikola Kasabov. Integrated feature and parameter optimization for an evolving spiking neural network: Exploring heterogeneous probabilistic models. *Neural Networks*, 22(5):623–632, 2009.

[44] Zhenzhong Wang, Lilin Guo, and Malek Adjouadi. A generalized Leaky Integrate-and-Fire neuron model with fast implementation method. *International journal of neural systems*, 24(5):1440004, 8 2014.

[45] Beata Strack, Kimberle M Jacobs, and Krzysztof J Cios. Simulating vertical and horizontal inhibition with short-term dynamics in a multi-column multi-layer model of neocortex. *International journal of neural systems*, 24(5):1440002, 8 2014.

[46] Claudia Casellato, Alberto Antonietti, Jesús A Garrido, Richard R Carrillo, Niceto R Luque, Eduardo Ros, Alessandra Pedrocchi, and Egidio D'Angelo. Adaptive Robotic Control Driven by a Versatile Spiking Cerebellar Network. *PLoS ONE*, 9(11):e112265, 11 2014.

[47] Christopher H Yeo and Germund Hesslow. Cerebellum and conditioned reflexes. *Trends in cognitive sciences*, 2(9):322–30, 9 1998.

[48] Selmaan N Chettih, Samuel D McDougle, Luis I Ruffolo, and Javier F Medina. Adaptive timing of motor output in the mouse: the role of movement oscillations in eyelid conditioning. *Frontiers in integrative neuroscience*, 5(November):72, 1 2011.

[49] Edward S Boyden, Akira Katoh, and Jennifer L Raymond. Cerebellum-dependent learning: the role of multiple plasticity mechanisms. *Annual review of neuroscience*, 27(1):581–609, 1 2004.

[50] David J Herzfeld, Damien Pastor, Adrian M Haith, Yves Rossetti, Reza Shadmehr, and Jacinta O'Shea. Contributions of the cerebellum and the motor cortex to acquisition and retention of motor memories. *NeuroImage*, 98:147–158, 2014.

[51] Jason R Pugh and Indira M Raman. Potentiation of mossy fiber EPSCs in the cerebellar nuclei by NMDA receptor activation followed by postinhibitory rebound current. *Neuron*, 51(1):113–23, 7 2006.

[52] Lisa Mapelli, Martina Pagani, Jesús A Garrido, and Egidio D'Angelo. Integrated plasticity at inhibitory and excitatory synapses in the cerebellar circuit. *Frontiers in Cellular Neuroscience*, 9(May):1–17, 2015.

[53] Egidio D'Angelo, Lisa Mapelli, Claudia Casellato, Jesús A Jesus A. Garrido, Niceto R Luque, Jessica Monaco, Francesca Prestori, Alessandra Pedrocchi, Eduardo Ros, Egidio D'Angelo, Lisa Mapelli, Claudia Casellato, Jesús A Jesus A. Garrido, Niceto R Luque, Jessica Monaco, Francesca Prestori, Alessandra Pedrocchi, and Eduardo Ros. Distributed Circuit Plasticity: New Clues for the Cerebellar Mechanisms of Learning. *The Cerebellum*, 15(2):139–151, 8 2015.

[54] Egidio D'Angelo, Sebastiaan K E Koekkoek, Paola Lombardo, Sergio Solinas, Eduardo Ros, Jesús A Garrido, Martijn Schonewille, and Chris I De Zeeuw. Timing in the cerebellum: oscillations and resonance in the granular layer. *Neuroscience*, 162(3):805–15, 9 2009.

[55] Fredrik Johansson, Hannes A.E. Carlsson, Anders Rasmussen, Christopher H. Yeo, and Germund Hesslow. Activation of a Temporal Memory in Purkinje Cells by the mGluR7 Receptor. *Cell Reports*, 13(9):1741–1746, 12 2015.

[56] G. Grimaldi, G. P. Argyropoulos, A. Boehringer, P. Celnik, M. J. Edwards, R. Ferrucci, J. M. Galea, S. J. Groiss, K. Hiraoka, P. Kassavetis, E. Lesage, M. Manto, R. C. Miall, A. Priori, A. Sadnicka, Y. Ugawa, and U. Ziemann. Non-invasive Cerebellar Stimulation—a Consensus Paper. *The Cerebellum*, 13(1):121–138, 2 2014.

[57] Massimiliano Oliveri, Giacomo Koch, Sara Torriero, and Carlo Caltagirone. Increased facilitation of the primary motor cortex following 1 Hz repetitive transcranial magnetic stimulation of the contralateral cerebellum in normal humans. *Neuroscience letters*, 376(3):188–93, 3 2005.

[58] B Fierro, A Palermo, A Puma, M Francolini, M L Panetta, O Daniele, and F Brighina. Role of the cerebellum in time perception: a TMS study in normal subjects. *Journal of the neurological sciences*, 263(1-2):107–12, 12 2007.

[59] Berthold Langguth, Dirk De Ridder, John L Dornhoffer, Peter Eichhammer, Robert L Folmer, Elmar Frank, Felipe Fregni, Christian Gerloff, Eman Khedr, Tobias Kleinjung, Michael Landgrebe, Scott Lee, Jean-Pascal Lefaucheur, Alain Londero, Renata Marcondes, Aage R Moller, Alvaro Pascual-Leone, Christian Plewnia, Simone Rossi, Tanit Sanchez, Philipp Sand, Winfried Schlee, Dipl Pysch, Thomas Steffens, Paul Van De Heyning, and Goeran Hajak. Controversy: Does repetitive transcranial magnetic stimulation/ transcranial direct current stimulation show efficacy in treating tinnitus patients? *Brain Stimulation*, 1:192–205, 2008.

[60] Andrew D. Pinto and Robert Chen. Suppression of the motor cortex by magnetic stimulation of the cerebellum. *Experimental Brain Research*, 140(4):505–510, 10 2001.

[61] Elise Lesage, Blaire E Morgan, Andrew C Olson, Antje S Meyer, and R Chris Miall. Cerebellar rTMS disrupts predictive language processing. *Current biology : CB*, 22(18):794–5, 9 2012.

[62] Andrew J Butler and Steven L Wolf. Putting the Brain on the Map: Use of Transcranial Magnetic Stimulation to Assess and Induce Cortical Plasticity of Upper-Extremity Movement. *Physical Therapy*, 87(6):719–736, 6 2007.

[63] Britt S Hoffland, Matteo Bologna, Panagiotis Kassavetis, James T H Teo, John C Rothwell, Christopher H Yeo, Bart P van de Warrenburg, and Mark J Edwards. Cerebellar theta burst stimulation impairs eyeblink classical conditioning. *The Journal of physiology*, 590(4):887–897, 2 2012.

[64] Philip J E Attwell, Samuel F Cooke, and Christopher H Yeo. Cerebellar Function in Consolidation of a Motor Memory. *Neuron*, 34(6):1011–1020, 6 2002.

[65] S. F. Cooke, Phillip J E Attwell, and Christopher H Yeo. Temporal Properties of Cerebellar-Dependent Memory Consolidation. *Journal of Neuroscience*, 24(12):2934–2941, 3 2004.

[66] Adrian M Haith and John W Krakauer. Theoretical models of motor control and motor learning. *Routledge handbook of motor control and motor learning. London: Routledge*, pages 7–28, 2013.

[67] Alice Geminiani, Claudia Casellato, Alberto Antonietti, Egidio D'Angelo, and Alessandra Pedrocchi. A Multiple-Plasticity Spiking Neural Network Embedded in a Closed-Loop Control System to Model Cerebellar Pathologies. *International journal of neural systems*, page S0129065717500174, 1 2017.

[68] Viktor Jirsa, Olaf Sporns, Michael Breakspear, Gustavo Deco, and Antony R McIntosh. Towards the virtual brain: network modeling of the intact and the damaged brain. *Archives italiennes de biologie*, 148(3):189–205, 9 2010.

[69] Erik De Schutter, Orjan Ekeberg, Jeanette Hellgren Kotaleski, Pablo Achard, and Anders Lansner. Biophysically detailed modelling of microcircuits and beyond, 2005.

[70] Lilin Guo, Zhenzhong Wang, Mercedes Cabrerizo, and Malek Adjouadi. A Cross-Correlated Delay Shift Supervised Learning Method for Spiking Neurons with Application to Interictal Spike Detection in Epilepsy. *International Journal of Neural Systems*, 27(03):1750002, 5 2017.

[71] Frank A Middleton and Peter L Strick. Cerebellar output channels. *International review of neurobiology*, 41:61–82, 1997.

[72] Mario Manto, James M Bower, Adriana Bastos Conforto, José M Delgado-García, Suzete Nascimento Farias da Guarda, Marcus Gerwig, Christophe Habas, Nobuhiro Hagura, Richard B. Ivry, Peter Mariën, Marco Molinari, Eiichi Naito, Dennis A. Nowak, Nordeyn Oulad Ben Taib, Denis Pelisson, Claudia D Tesche, Caroline Tilikete, and Dagmar Timmann. Consensus Paper: Roles of the Cerebellum in Motor Control—The Diversity of Ideas on Cerebellar Involvement in Movement. *The Cerebellum*, 11(2):457–487, 6 2012.

[73] Markus Thurling, Fabian Kahl, Stefan Maderwald, Roxana M Stefanescu, Marc Schlamann, Henk-Jan Boele, Chris I De Zeeuw, Jorn Diedrichsen, Mark E Ladd, Sebastian K E Koekkoek, and Dagmar Timmann. Cerebellar Cortex and Cerebellar Nuclei Are Concomitantly Activated during Eyeblink Conditioning: A 7T fMRI Study in Humans. *Journal of Neuroscience*, 35(3):1228–1239, 2015.

[74] Alberto Antonietti, Claudia Casellato, Jesús A Garrido, Egidio D'Angelo, and Alessandra Pedrocchi. Spiking cerebellar model with multiple plasticity sites reproduces eye blinking classical conditioning. In *2015 7th International IEEE/EMBS Conference on Neural Engineering (NER)*, volume 2015-July, pages 296–299. IEEE, 4 2015.

[75] Richard R Carrillo, Eduardo Ros, Christian Boucheny, and Olivier J M D Coenen. A real-time spiking cerebellum model for learning robot control. *Biosystems*, 94(1):18–27, 2008.

[76] Javier F Medina, Keith S Garcia, William L Nores, Nichole M Taylor, and Michael D Mauk. Timing mechanisms in the cerebellum: testing predictions of a large-scale computer simulation. *The Journal of Neuroscience*, 20(14):5516–25, 7 2000.

[77] Mathilde Badoual, Quan Zou, Andrew P Davison, Michael Rudolph, Thierry Bal, Yves Frégnac, and Alain Destexhe. Biophysical and phenomenological models of multiple spike interactions in spike-timing dependent plasticity. *International journal of neural systems*, 16(2):79–97, 4 2006.

[78] Sou Nobukawa and Haruhiko Nishimura. Enhancement of Spike-Timing-Dependent Plasticity in Spiking Neural Systems with Noise. *International Journal of Neural Systems*, 26(05):1550040, 8 2016.

[79] Felix Weissenberger, Florian Meier, Johannes Lengler, Hafsteinn Einarsson, and Angelika Steger. Long Synfire Chains Emerge by Spike-Timing Dependent Plasticity Modulated by Population Activity. *International Journal of Neural Systems*, 27(08):1750044, 12 2017.

[80] Jesús A. Garrido, Niceto R. Luque, Silvia Tolu, and Egidio D'Angelo. Oscillation-Driven Spike-Timing Dependent Plasticity Allows Multiple Overlapping Pattern Recognition in Inhibitory Interneuron Networks. *International Journal of Neural Systems*, 26(05):1650020, 8 2016.

Learning rule mechanisms of the model The SNN model was equipped with three plasticity sites, cortical and nuclear. The synaptic connections in each site followed three different learning rules, which strengthen or weaken these connections. Long-Term Depression (LTD) or Long-Term Potentiation (LTP) mechanisms were modeled as modifications on the synaptic conductances [74, 20].

The 1st learning rule models the LTP-LTD at the cerebellum cortical level (PF-PC) [32].

$$\Delta W_{PF_i \to PC_j}(t) = \begin{cases} LTD_1 \int_{-\infty}^{t_{IOspike_j}} K_1(t-x)\delta_{PF_i}(t-x)\mathrm{d}x & \text{if } PC_j \text{ active} \\ & t = t_{IOspike_j} \\ LTP_1 & \text{if } PC_j \text{ active} \\ & t \neq t_{IOspike_j} \\ 0 & \text{otherwise} \end{cases} \tag{1}$$

where:

$$\delta_{PF_i}(s) = \begin{cases} 1 & \text{if } PF_i \text{ is active at time } s \\ 0 & \text{otherwise} \end{cases} \tag{2}$$

and the Kernel function is:

$$K_1(z) = A\mathrm{e}^{-\frac{z-t_0}{\tau}} \left(sin\left(2\pi \frac{z-t_0}{\tau}\right)\right)^{20} \tag{3}$$

where LTD_1 and LTP_1 are the first learning rule constants; $t_{IOspike_j}$ is the time when the corresponding CF_j emits a spike; $K_1(z)$ is the integral kernel function, which has its peak at t_0 (100 ms) before $t_{IOspike_j}$; τ and A are normalization constants. LTD_1 and LTP_1 values were defined by the optimization process. The rationale of the kernel function is presented in detail in [75].

The 2nd learning rule regards the MF-DCN nuclear connections [76].

$$\Delta W_{MF_i \to DCN_j}(t) = \begin{cases} LTD_2 \int_{-\infty}^{+\infty} K_2(t-x)\delta_{MF_i}(t-x)\mathrm{d}x & \text{if } MF_i \text{ active} \\ & t = t_{PCspike_j} \\ LTP_2 & \text{if } PC_j \text{ active} \\ & t \neq t_{PCspike_j} \\ 0 & \text{otherwise} \end{cases} \tag{4}$$

where:

$$\delta_{MF_i}(s) = \begin{cases} 1 & \text{if } MF_i \text{ is active at time } s \\ 0 & \text{otherwise} \end{cases} \tag{5}$$

and the Kernel function is:

$$K_2(z) = \mathrm{e}^{-\frac{|z|}{\tau}} \left(cos\left(\frac{z}{\tau}\right) \right)^2 \tag{6}$$

where LTD_2 and LTP_2 are the first learning rule constants; $t_{PCspike_j}$ is the time when the corresponding PC_j emits a spike; $K_2(z)$ is the integral kernel function and τ is used in order to normalize the arguments in the learning rule. LTD_2 and LTP_2 values were defined by the optimization process made by the GA.

The 3$^{\text{rd}}$ learning rule regards the PC-DCN nuclear connections and it was implemented as a standard Spike-Timing Dependent Plasticity (STDP) [77, 78, 79, 80]. Considering the i$^{\text{th}}$ DCN (DCN$_{\text{i}}$) and the two PCs connected with this DCN:

when one of the two PCs fires and, within a LTP-time window equal to 20 ms, also the DCN_i fires, the two inhibitory synapses from PCs to DCN_i are increased. The amount of conductance increase depends on the delay between PC and DCN spikes, with a maximum LTP change equal to LTP_3

when the DCN_i emits a spike and, within a LTD-time window equal to 50 ms, also one of the two PCs fires, the two PC-DCN connections are decreased. The amount of conductance decrease depends on the delay between DCN and PC spikes, with a maximum LTD change equal to LTD_3.

Genetic Algorithm details To select the parameters of the model which were producing a behavior (i.e. CR%) as much similar as possible to the human data, we aimed at maximizing the fitness function defined by equation (7):

$$\begin{aligned} fitness = \\ \Bigg[\left(1 - \frac{\sum_{i=1}^{22} |CR\%_{exp}(i) - CR\%_{mod}(i)|}{22}\right) \cdot \frac{2}{5} + \\ + \left(1 - \frac{\sum_{i=23}^{66} |CR\%_{exp}(i) - CR\%_{mod}(i)|}{44}\right) \cdot \frac{1}{5} + \\ + \left(1 - \frac{\sum_{i=67}^{77} |CR\%_{exp}(i) - CR\%_{mod}(i)|}{11}\right) \cdot \frac{2}{5} \Bigg] \cdot \\ \cdot \left(1 - \frac{\sum_{i=1}^{77} OUT(i)}{77}\right) \end{aligned} \tag{7}$$

where $CR\%_{exp}(i)$ was the CRs percentage (computed over a time-window of 10 trials) of the median of experimental data at the i$^{\text{th}}$ trial; $CR\%_{mod}(i)$ was the CRs percentage of the model at the i$^{\text{th}}$ trial. The fast phases of acquisition and extinction (trials 1-22 and 67-77, respectively) were weighted more than the plateau (trials 23-66), since they were the most critical phase. The last multiplying member, containing $OUT(i)$, penalized the fitness if the CR% of the model at the i$^{\text{th}}$ trial was outside the interquartile interval of the human data. If, at the i$^{\text{th}}$ trial, the $CR\%_{mod}$ was included within the quartiles of $CR\%_{exp}$, $OUT(i)$ was set to 0, otherwise it was set to 1.

When the model behavior coincided with the median of experimental data, the value of the fitness function reached its maximum (i.e. 1), it decreased along with the dissimilarity between the model behavior and the experimental one.

At the end of each generation, the GA kept the best 4 individuals as they were (elitism), and then performed three operations to generate the other 8 individuals of the following generation (12 individuals for each generation). The first operation was the selection process, made by the roulette wheel method: the individuals of the current generation had a probability of becoming the parents of individuals of the following generation proportional to their fitness score. As a result of the selection process, 8 individuals were chosen as parents. Then, each pair of parents had a probability of 80% to perform a crossover, which consisted into swapping 4 random genes. The third operation was the mutation, each individual had a 90% probability of a mutation to 5 genes, whose values could be re-extracted within their ranges or increased/decreased from their current value with a Gaussian distribution function. The new 12 individuals generated by the GA were then simulated. The optimization process continued as long as one of the stopping criteria was satisfied: 1000 generation were tested or the fitness function increase between two generations was lower than 0.1% for 100 consecutive generations.

Table 1: Results of GA optimization and statistical comparison of CR numbers between models and experimental data, for each group and each phase (Early Acquisition, Late Acquisition, and Extinction). *p-values* are reported for each comparison (12 Wilcoxon rank sum tests).

Groups	Num gen	Max fit	EA	LA	EX
ALL-PRE	301	0.95	0.013	0.262	$\sim 10^{-5}$
SHAM-POST	275	0.91	$\sim 10^{-5}$	0.516	0.596
RIGHT-POST	290	0.87	0.094	0.076	0.444
LEFT-POST	135	0.90	0.131	0.767	0.213

Table 2: Statistical comparison of CR rates between models and experimental data, for each group and each phase (Early Acquisition, Late Acquisition, and Extinction). *p-values* are reported for each comparison (Kruskall-Wallis and Multiple Comparison with Bonferroni correction).

$0 \rightarrow EA$	ALL PRE	SHAM POST	RIGHT POST	LEFT POST
ALL-PRE	==	$8.7\,10^{-70}$	$4.8\,10^{-27}$	$3.5\,10^{-6}$
SHAM-POST	$8.7\,10^{-70}$	==	$2.6\,10^{-19}$	$3.8\,10^{-23}$
RIGHT-POST	$4.8\,10^{-27}$	$2.6\,10^{-19}$	==	0.003
LEFT-POST	$3.5\,10^{-6}$	$3.8\,10^{-23}$	0.003	==
$EA \rightarrow LA$	ALL PRE	SHAM POST	RIGHT POST	LEFT POST
ALL-PRE	==	$1.9\,10^{-52}$	$2.7\,10^{-18}$	$4.9\,10^{-32}$
SHAM-POST	$1.9\,10^{-52}$	==	$1.4\,10^{-16}$	1.00
RIGHT-POST	$2.7\,10^{-18}$	$1.4\,10^{-16}$	==	$6.1\,10^{-8}$
LEFT-POST	$4.9\,10^{-32}$	1.00	$6.1\,10^{-8}$	==
$LA \rightarrow EX$	ALL PRE	SHAM POST	RIGHT POST	LEFT POST
ALL-PRE	==	0.060	$2.0\,10^{-6}$	$7.4\,10^{-14}$
SHAM-POST	0.060	==	0.15	$1.4\,10^{-7}$
RIGHT-POST	$2.0\,10^{-6}$	0.15	==	0.0001
LEFT-POST	$7.4\,10^{-14}$	$1.4\,10^{-7}$	0.0001	==

A standard desktop PC (Intel Core i7-2600 CPU @3.40 GHz with 8 GB of RAM with Windows 7 64 bit) was used to carry out the simulations, exploiting its 4 cores to run multiple simulations in parallel.

Table 3: Cumulative weight change slopes in sessions-2 for the three plasticities.

PF-PC ($\times 10^4$)	m1	m2	m3	m4	m5	m6	m7
SHAM-POST	-10.8	-1.1	0.04	-0.5	-0.3	-0.1	5.5
RIGHT-POST	-10.4	-0.6	-0.05	0.02	0.03	0.03	7.8
LEFT-POST	-10.4	-0.4	0.02	-0.1	-0.01	-0.09	8.8
MF-DCN							
SHAM-POST	0.54	1.08	1.10	1.11	1.12	1.13	1.08
RIGHT-POST	1.30	2.42	2.42	2.43	2.43	2.43	2.39
LEFT-POST	1.53	2.82	2.82	2.82	2.83	2.83	2.79
PC-DCN ($\times 10^{-3}$)							
SHAM-POST	0.4	2.0	1.3	1.4	1.9	1.5	1.4
RIGHT-POST	-3.5	-6.8	-6.9	-6.9	-6.7	-6.8	-6.9
LEFT-POST	-1.6	-3.8	-3.5	-3.7	-3.5	-3.3	-3.7